Structural Eng. / Earthquake Eng. Vol. 7. No. 1, 77s-87s. April 1990
Japan Society of Civil Engineers (Proc. of JSCE No. 416/I-13)

ANALYSIS OF STRESS WAVE PROPAGATION IN COMPOSITE RECTANGULAR BEAM IN THE CASE OF ULTRASONIC PULSE METHOD

By Toshiyuki OSHIMA, Shuichi MIKAMI** and Sumio G. NOMACHI****

Elastodynamic behavior of a two-dimensional composite rectangular beam, which has regularly-spaced fibers, is formulated by a couple of finite difference equation based on FEM formulation of rectangular element. Making use of modal analysis and Duhamel integral equation, the impulse response of the composite rectangular beam is obtained. The transient response from the first incident wave through the whole oscillation of the beam is found by the series of simulation analysis. The effects of coupling oscillation of the transducer and the beam on the impulse response of incident stress wave are obtained in experiments of the ultrasonic pulse method. In addition, the effect of internal friction of the beam and the frequency dependence of damping coefficient are discussed.

Keywords: *stress wave, ultrasonic wave, diagnosis, NDE*

1. INTRODUCTION

The recent demand for more reliable diagnosis of structural integrity needs to improve analyzing methods for stress wave propagation, diffraction, and reflection measured by an ultrasonic pulse method. Setting up the accurate diagnosis of structural integrity, we are able to estimate the practical remaining life time of the structure.

The stress wave, which propagates in a beam of rectangular section, disperses on account of its finite size of section. Reinforcing fibers in an elastic matrix also cause the dispersion of stress wave on another account. The aim of the present paper is to find how these dispersion effects are associated with the impulse response of the composite beam of rectangular section and more specially is to clarify how the stress wave propagates in the rectangular composite beam in case of ultrasonic pulse method. Studies in respect to the analysis of stress wave propagation in the structure may be classified in two parts; the one is the study on ultrasonic flaw detection and the other on acoustic emission (AE) method. The former is mainly applied to the flaw detection of welding and debonding detection in fiber reinforced composite, and the latter plays an important role in the field of nondestructive inspection[1)~3)]. Equipments recently developed make it possible to measure the detail scattering of stress wave in the structure, and that much work has been published by many researchers[4),5)]. First of all, the transmitting response from the initial impulse at the surface of the structure has to be found out as well as accompanying damping effects on it. Formulating

* Member of JSCE, Dr. Eng., Associate Professor, Department of Development Engineering, Kitami Institution of Technology (165 Koencho, Kitami, 090)
** Member of JSCE, Technical Official, Department of Development Engineering, Kitami Institute of Technology (165 Koencho, Kitami, 090)
*** Member of JSCE, Dr. Eng., Professor, Department of Civil Engineering, College of Industrial Technology, Nihon University (1-2-1 Izumi, Narashino, Chiba, 275)

a couple of finite difference equations for a two-dimensional beam and analyzing ultrasonic response due to impulsive pulse by means of the modal analysis, we well find the process of transient response from the first incident time through the remainder portion by series of simulation analysis.

Characteristics of the incident wave induced by ultrasonic pulse at the surface of the beam are related with the impedance ratio between a transducer and a beam, the modal trait of the transducer, and the contact pressure from transducer to beam. In addition, the shape of stress wave may change during the propagating process due to the internal friction of the beam. The above all aspects are clarified in the following analysis.

2. DYNAMIC RESPONSE OF COMPOSITE RECTANGULAR BEAM

A two dimensional composite rectangular beam is shown in Fig. 1. The beam has regularly-spaced fibers perpendicular to x-y plane, namely in the z direction. The effect of the fibers in the z direction can be neglected in the case of taking into account stress wave propagating only in the xy plane.

The span of the beam l is devided into M elements of λ_2 in the horizontal direction and the depth h into N elements of λ_3 in the vertical direction.

FEM formulation for two dimensional rectangular element is obtained by means of Galerkin's method, employing the displacement distribution with linear variation in the element,

$$\int_A L_1\left(\frac{\partial \sigma_x}{\partial x}+\frac{\partial \tau_{xy}}{\partial y}-\rho\frac{\partial^2 u}{\partial t^2}\right)dA=0 \cdots\cdots (1)$$

$$\int_A L_2\left(\frac{\partial \tau_{xy}}{\partial x}+\frac{\partial \sigma_y}{\partial y}-\rho\frac{\partial^2 v}{\partial t^2}\right)dA=0 \cdots\cdots (2)$$

where L_1 and L_2 are the shape function of rectangular element and A is the area of the element. Considering the equilibrium at the node (x, y) and the mass forces of the fiber in two directions of x and y, we obtain simultaneous difference equations.

$$\frac{(2\mu+\lambda)\lambda_3}{6\lambda_2}\Delta_x^2\bar{\Delta}_y^2 u_{xy}+\frac{\mu\lambda_2}{6\lambda_3}\bar{\Delta}_x^2\Delta_y^2 u_{xy}+\frac{\mu+\lambda}{4}\Delta_x\Delta_y v_{xy}=\frac{\rho\lambda_2\lambda_3}{36}\bar{\Delta}_x^2\bar{\Delta}_y^2 u''_{xy}+\rho_f A_f u''_{xy} \cdots\cdots (3)$$

$$\frac{\mu+\lambda}{4}\Delta_x\Delta_y v_{xy}+\frac{(2\mu+\lambda)\lambda_2}{6\lambda_3}\Delta_x^2\bar{\Delta}_y^2 v_{xy}+\frac{\mu\lambda_3}{6\lambda_2}\bar{\Delta}_x^2\Delta_y^2 v_{xy}=\frac{\rho\lambda_2\lambda_3}{36}\bar{\Delta}_x^2\bar{\Delta}_y^2 v''_{xy}+\rho_f A_f v''_{xy} \cdots\cdots (4)$$

where μ and λ are Lame's elastic constants, and notations as follow;

$$\Delta_x^2 fx=f(x+1)-2f(x)+f(x-1),\quad \Delta_x fx=f(x+1)-f(x-1),\quad \bar{\Delta}_x^2 fx=\Delta_x^2 fx+6fx,\quad f'=\frac{\partial f}{\partial t}.$$

ρ is density of matrix, ρ_f and A_f are the density and the sectional area of fiber, respectively.

Making use of Finite Integration Transform (FIT)[6),12)] with respect to regularly-spaced discrete coordinate, Eqs. (3) and (4) are transformed into the matrix expression.

In order to compare the results by using FIT with the equations of Finite Strip Method (FSM)[8)] for the layered beam as shown Fig. 2, the matrix elements concerning to y-th layer are obtained as follows;

$$\begin{bmatrix} a_{11} & a_{12} & a_{13} & a_{14} \\ & a_{22} & a_{23} & a_{24} \\ \text{Sym.} & & a_{33} & a_{34} \\ & & & a_{44} \end{bmatrix}\begin{Bmatrix} \bar{u}_{my} \\ \bar{v}_{my} \\ \bar{u}_{my+1} \\ \bar{v}_{my+1} \end{Bmatrix}=\begin{bmatrix} b_{11} & 0 & b_{13} & 0 \\ & b_{22} & 0 & b_{24} \\ \text{Sym.} & & b_{33} & 0 \\ & & & b_{44} \end{bmatrix}\begin{Bmatrix} \bar{u}''_{my} \\ \bar{v}''_{my} \\ \bar{u}''_{my+1} \\ \bar{v}''_{my+1} \end{Bmatrix}\frac{1}{\lambda_2^2\lambda_3} \cdots\cdots (5)$$

where

$$a_{11}=-\frac{2\mu+\lambda}{3\lambda_2^2}\lambda_3 D_m-\frac{\mu}{6\lambda_3}(6-D_m),\quad a_{12}=\frac{\mu-\lambda}{2\lambda_2}\sin\frac{m\pi}{M},$$

$$a_{13}=-\frac{2\mu+\lambda}{6\lambda_2^2}\lambda_3 D_m+\frac{\mu}{6\lambda_3}(6-D_m),\quad a_{14}=\frac{\mu+\lambda}{2\lambda_2}\sin\frac{m\pi}{M},$$

$$a_{22}=-\frac{2\mu+\lambda}{6\lambda_3}(6-D_m)-\frac{\mu\lambda_3}{3\lambda_2^2}D_m,\quad a_{24}=\frac{2\mu+\lambda}{6\lambda_3}(6-D_m)-\frac{\mu\lambda_3}{6\lambda_2^2}D_m,$$

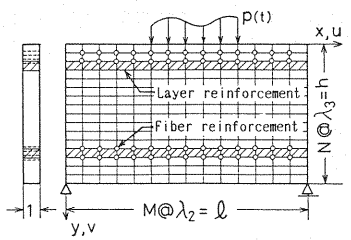

Fig. 1 Composite rectangular beam.

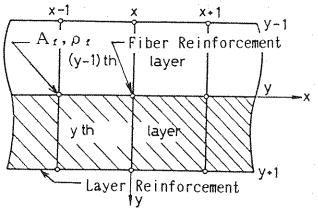

Fig. 2 Coordinates.

$$a_{23}=-a_{14},\quad a_{33}=a_{11},\quad a_{34}=-a_{12},\quad a_{44}=-\frac{2\mu+\lambda}{6\lambda_3}(6-D_m)-\frac{\mu\lambda_3}{6\lambda_2^2}D_m,$$

$$b_0=\frac{\rho}{36}\lambda_3(6-D_m),\quad b_{11}=b_{22}=b_{33}=b_{44}=2b_0+\frac{\rho_f A_f}{2\lambda_2},\quad b_{13}=b_{24}=b_0,\quad D_m=2\left(1-\cos\frac{m\pi}{M}\right)$$

$\overline{u}_m$ and $\overline{v}_m$ are Fourier coefficients of the displacements u and v, respectively[6),12)].

Superposing the equations like Eq. (5) for all elements of the beam and the effect of point mass forces of the fibers, we obtain the following dynamic equation of composite rectangular beam,

$$[K]\{\delta_{st}\}+[M]\{\delta''_{st}\}=\{F_{st}\} \quad (6)$$

where $[K]$=stiffness matrix, $[M]$=mass matrix, $\{\delta_{st}\}$=displacement vector, and $\{F_{st}\}$=external force vector for the whole structure of the beam shown in Fig. 1, respectively. And adding the damping matrix $[C]$, Eq. (6) yields

$$[M]\{\delta''_{st}\}+[C]\{\delta'_{st}\}+[K]\{\delta_{st}\}=\{F_{st}\} \quad (7)$$

Making use of modal analysis and Duhamel integral equation for Eq. (7), the impulse response of the composite rectangular beam is obtained.

3. CHARACTERISTICS OF INCIDENT WAVE INDUCED BY PIEZOELECTRIC TRANSDUCER

To analyze accurately the impulse response of the beam and the effect of inclusion and damping in oscillating beam by using the ultrasonic pulse method, first we need to know the incident waveform driven into the beam. Then, the deformation process of the incident wave by the inclusion and damping during the propagation has to be analyzed. In the theoretical analysis the incident wave applied is taken into account as the input data for the external force to calculate Duhamel integral equation given by modal analysis of Eq. (7), by which we can estimate the effects of inclusion and internal damping on the waveform. For this purpose we detect incident impulsive waves by using the experimental equipments and analyze the effects of (1) impedance ratio between a transducer and a solid body, (2) natural frequencies of the transducer, and (3) the contact pressure of the transducer to the body, respectively. The experimental equipments as shown in Fig. 3 are used to obtain the surface response at an induced point of the body. In this experiment, the stress wave is obtained passing through the filter of each equipment. Therefore, we, in advance, need to obtain the characteristics of frequency response of the filter and then make some corrections on the received stress wave if it is necessary. To record the incident wave just at an applied location we employ a set of transducers consisting of a hollow-type and a solid-cylinder, as shown in Fig. 4.

(1) Comparison of incident wave characteristics in steel and mortar

Using steel and mortar specimens, the coupling oscillation with the piezoelectric transducer on the surface of the body is measured. By putting the set of transducer and receiver on the body as shown in Fig. 4, the impulses with different duration are induced through the transducer. The natural frequency of hollow type transducer is around 50 kHz and it generates the incident surface dilatational wave of different peak frequencies by changing the duration time of the step pulse. The induced oscillation is formulated as dynamic force applied in a half infinite body at the hollow type transducer. Thus the peak frequencies in the

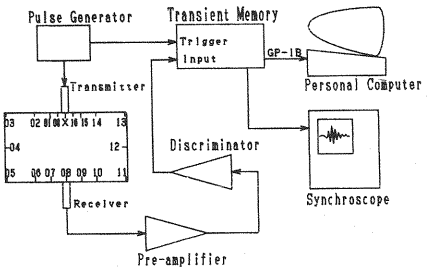

Fig. 3 Block diagram.

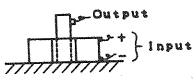

Fig. 4 The set of transducers with hollow and solid cylinder.

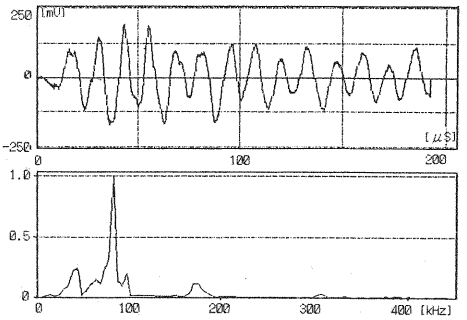

Fig. 5 Incident surface waveform and its spectrum on steel.

spectrum are coincident with the frequency of the coupling oscillation and its natural frequency of the transducer. In Fig. 5 and Fig. 6 the incident waves detected and their spectra on the steel and mortar specimens are shown.

(2) Analysis of oscillation of transducer

Experimental results obtained by different natural frequencies of the transducer are discussed. Although the transducer has own natural frequencies and damping coefficients, the coupling effect between the transducer and the beam also provide another oscillation. To know the coupling effect between the transducer and the beam including its damping effect at the resonance frequencies, we analyzed the experimental results of dynamic response. That is, we analyzed the responses of a simple system of transducers. This system is made of two transducers with natural frequencies of arround 150 kHz which are put face to face and one is used for transducer and another for receiver. We call here this system as "sensor-to-sensor" model. One of the response of sensor-to-sensor model is shown in Fig. 7. From the figures it is observed that the frequency at the highest peak in the spectrum coincides with the own natural frequency of sensors. We find if we take the sensor with 150 kHz as a transducer, the response of the coupling oscillation appeares arround at 75 kHz as a total response of the model. As we can formulate the response of this model as a combination of the systems of one-degree of freedom and determine its modal parameters, the transient coupling oscillation induced by impulsive electric step pulse of duration time ΔT and its total pressures $F=EA\varepsilon$ (where ε : piezoelectric strain), will be numerically obtained by comparing with the experimental results.

(3) Effect of contact pressure between transducer and beam

The effect of the contact area and the contact pressure of transducer to the solid body is not neglectable in the coupling oscillation at the surface of the body. Before analyzing the dynamic response of incident

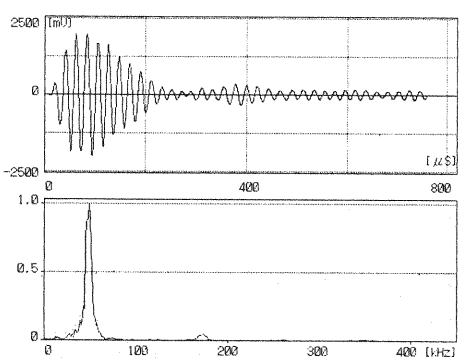

Fig. 6 Incident surface waveform and its spectrum on mortar.

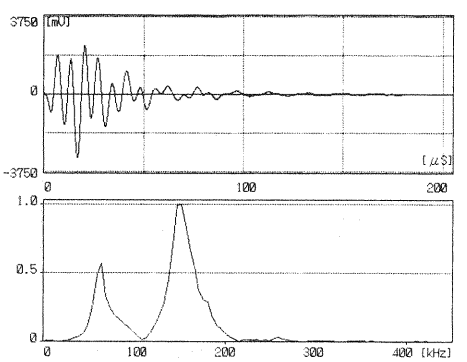

Fig. 7 The response of sensor-to-sensor model.

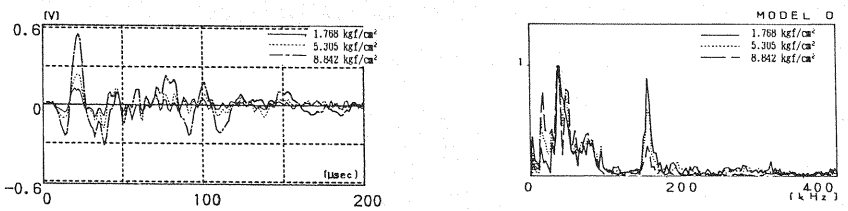

(a) wave form (b) spectrum

Fig. 8 Comparison of surface response at induced point with three cases of contact pressure.

stress wave propagating in a composite rectangular beam, we have to pay our attention to the effect of loading area on the upper side of the beam. The dynamic responses of displacement and velocity at the span center of the upper side in the uniform rectangular beam as shown in Fig. 1 are compared among three cases of the ratio $2c/l$ of loaded length and total span length; 0, 2/70, 4/70. The duration time of incident step pulse is taken as 50 μs. From the numerical results we find that the effect of contact area on the surface response will be small in the comparison between theoretical and experimental results.

In order to analyze the effect of contact pressure of the transducer to the surface of the body, special sensing devices of a transducer and a receiver are used for the measurement of the contact pressure and the dynamic responses of the body in several cases are obtained. In this experiment, the mortar specimen is used as a oscillating solid and the contact pressure is measured through highly sensitive transducer and put in digital memory together with the incident and received stress waves in the solid. The pressures of transducer and receiver are taken as nearly equal in every measurement. In Fig. 8 the surface responses of the mortar at the induced point and their spectra are compared among three cases of contact pressure; 1.768 kgf/cm^2, 5.305 kgf/cm^2 and 8.842 kgf/cm^2. Thus the higher the contact pressure becomes, the larger the maximum amplitude of the response becomes, decreasing the response of higher frequency component.

Then in order to compare between theoretical and experimental responses including the higher frequency component, it is important for contact pressure to take to be constant in every experiment.

4. DAMPING CHARACTERISTICS OF STRESS WAVE BY INTERNAL FRICTION

There is, on another account, a damping effect of the internal friction on the waveform analysis in the case of ultrasonic pulse method. That is, how to determine the damping coefficient in the calculation of modal analysis.

As elastic strain energy always change at a certain amount due to heat energy during the stress wave propagation, this behavior should be expressed by a damping effect due to internal friction. The damping effect by internal friction depends upon the amplitude and frequency of the oscillation. The amplitude of the stress wave in the ultrasonic pulse method is so small that the discussion is focused on the frequency dependence of the damping effect. A general aspect of the frequency dependence is possiblly shown in Fig. 9[9]. The dynamic response of granular materials like concrete, which consists of sand, cement, void, and water, is always anisotropic and complicated in the analytical aspects. As for the temperature over each constituent the small amount of heat may flow across the boundary of the element. The frequency dependence of damping effect by heat conduction during the oscillation has a lower bound as shown in Fig. 9. The deformation occurs slowly around this lower bound frequency, the volume may change isothermally, and then little energy loss takes place. This case is in much lower frequency[9].

On the other hand there is an upper bound frequency. At this frequency the deformation occurs so fast that there is no time for the heat to flow during the oscillation, and then little energy loss takes place. Thus the maximum energy loss may occur in the frequency between these two bounds. The bounds depend upon the size of the element of granular materials and other surrounding environment[9].

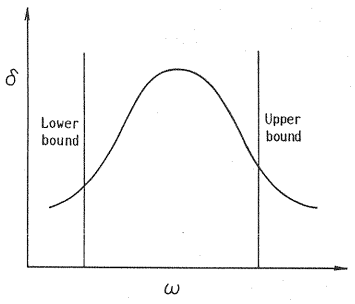

Fig. 9 General aspect of frequency dependence of logarithmic damping coefficient.

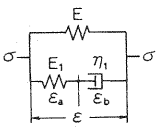

Fig. 10 Three element viscoelastic model.

Table 1 Mortar models with different weight (volume) ratios of water, cement and sand.

w/c	w	c	s
35% Model 0	0.35 (0.10)	1.0 (1.0)	0.95 (1.14)
50% Model L	0.50 (1.57)	1.0 (1.0)	2.0 (2.09)
65% Model P	0.65 (2.02)	1.0 (1.0)	2.52 (3.02)

(1) Consideration of the internal friction[9),10)]

As the frequency dependence aspect of logarithmic damping is shown in Fig. 9, the same type of frequency dependence can be obtained analytically by using a viscoelastic model of three elements as shown in Fig. 10. The equilibrium of stress and strain in Fig. 10 becomes,

$$\varepsilon_a+\varepsilon_b=\varepsilon, \quad \sigma=E\varepsilon+E_1\varepsilon_a, \quad E_1\varepsilon_a=\eta_1\dot{\varepsilon}_b \cdots\cdots (8)$$

and we assume

$$\varepsilon=\bar{\varepsilon}\sin\omega t$$
$$\varepsilon_a=\bar{\varepsilon}_a\sin(\omega t+\alpha) \cdots\cdots (9)$$
$$\varepsilon_b=\bar{\varepsilon}_b\sin(\omega t+\alpha)$$

where ω is the induced frequency of stress wave and

$$\tan\alpha=-\bar{\varepsilon}_a/\bar{\varepsilon}_b=\omega\eta_1/E_1 \cdots\cdots (10)$$

On the other hand, we have the relationship between logarithmic damping δ and $\tan\alpha$[9)], as follows;

$$\tan\alpha=\delta/\pi=2h_r\omega/\gamma_r \cdots\cdots (11)$$

where γ_r is the real part of damping natural frequency, and h_r is damping coefficient, respectively.

Thus, we have a relationship between stress and strain,

$$\sigma=\varepsilon(E+E_1\cos^2\alpha)\sin\omega t+\frac{1}{2}\varepsilon E_1\sin^2\alpha\cos\omega t \cdots\cdots (12)$$

The phase shift in Eq. (12) (and then the internal damping) is obtained as follows;

$$\tan\bar{\alpha}=\frac{K_E\tan\alpha}{1+K_E+\tan^2\alpha}, \text{ where } K_E=E_1/E \cdots\cdots (13)$$

(2) Experiment relating to internal friction

In order to investigate the phase shift by internal friction we made three rectangular beam models of mortar. These mix proportions are shown in Table 1. The dimension of the beam is of 70 cm length, 40 cm height, and 3 cm thickness. The water cement ratios w/c are 35 % (Model O), 50 % (Model L), and 65 % (Model P), respectively. The upper numbers in Table 1 indicate the weight ratios of the mix and the lower numbers are the volume ratios. The ratio of sand in this case becomes greater in order O, L, and P. The experimental equipment is same as shown in Fig. 3 and the responses of stress wave are measured at the same point of the side of each beam model. The comparison of received stress wave among three models are shown in Fig. 11. We can find out that when w/c becomes larger and then the ratio of sand and water becomes larger comparing with the ratio of cement, the phase shift of the stress wave becomes larger.

(3) Experimental results of frequency dependence on damping coefficient

In order to investigate the frequency dependence on damping coefficient, experimental results are obtained for three models as shown in Table 1 by using different transducers of different resonance frequencies. We determined the damping coefficient h_r by half-power method[11)] applied to the detected

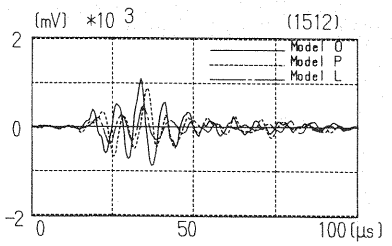

Fig. 11 Comparison of phase shift of stress wave with three models on the upper side of the beam.

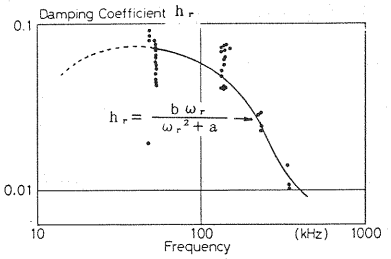

Fig. 12 Frequency dependence of damping coefficient.

stress wave which have approximately only one peak of frequency in spectrum. The results of frequency dependence on damping coefficient in the cases of three models O, L and P are shown in Fig. 12. Although this figure does not show the peak value, we can obtain the frequency dependence characteristics of the damping coefficient which is used to simulate by modal analysis as follows;

$$h_r=\frac{b\omega_r}{\omega_r^2+a} \quad \cdots\cdots (14)$$

where $a=13\,935$ and $b=15.52$.

5. NUMERICAL RESULTS OF IMPULSIVE RESPONSE AND SIMULATION

(1) Comparision with the equations of FSM

The effect of mesh number in the vertical direction y on the phase velocity is already known[7]. The phase velocity depends on the parameter $\alpha=h/l_s$ (h, l_s=height of the beam and length of the traveling stress wave). Thus it is better to take division number with α. There are, however, many adjacent values of natural frequency in each wave mode, it is not always necessary to take a small division length λ_3 to calculate the dynamic response of the beam. The concerning numerical results of the response will be shown later. It is also necessary to determine the division length λ_2 in the longitudinal direction for the accurate results, which are obviously related to the ratio between λ_2 and stress wave length l_s. In order to compare the result obtained by FIT using Eq. (5) with the results of Finite Strip Method (FSM)[8], the matrix elements for y-th finite strip layer in Fig. 2, as similar to Eq. (5), are given as follow;

$$a_{11}=-\frac{2\mu+\lambda}{3\lambda_2^2}\lambda_3\left(\frac{m\pi}{M}\right)^2-\frac{\mu}{\lambda_3},\quad a_{12}=\frac{\mu-\lambda}{2\lambda_2}\left(\frac{m\pi}{M}\right),\quad a_{13}=-\frac{2\mu+\lambda}{6\lambda_2^2}\lambda_3\left(\frac{m\pi}{M}\right)^2+\frac{\mu}{\lambda_3},$$

$$a_{14}=\frac{\mu+\lambda}{2\lambda_2}\left(\frac{m\pi}{M}\right),\quad a_{22}=-\frac{2\mu+\lambda}{\lambda_3}-\frac{\mu\lambda_3}{6\lambda_2^2}\left(\frac{m\pi}{M}\right)^2,\quad a_{23}=-a_{14},$$

$$a_{24}=\frac{2\mu+\lambda}{\lambda_3}-\frac{\mu\lambda_3}{3\lambda_2^2}\left(\frac{m\pi}{M}\right)^2,\quad a_{33}=a_{11},\quad a_{34}=-a_{12},\quad a_{44}=a_{22},\quad b_0=\frac{\rho\lambda_3}{6},$$

$$b_{11}=b_{22}=b_{33}=b_{44}=2b_0+\frac{\rho_f A_f}{2\lambda_2},\quad b_{13}=b_{24}=b_0$$

Taking the expansion theorem

$$D_m=\left(\frac{m\pi}{M}\right)^2-\frac{1}{12}\left(\frac{m\pi}{M}\right)^4+\frac{1}{360}\left(\frac{m\pi}{M}\right)^6-\cdots\cdots$$

$$\sin\left(\frac{m\pi}{M}\right)=\left(\frac{m\pi}{M}\right)-\frac{1}{6}\left(\frac{m\pi}{M}\right)^3+\frac{1}{120}\left(\frac{m\pi}{M}\right)^5-\cdots\cdots \quad \cdots\cdots (15)$$

we can see that the consideration of division number M in case of FIT has the same meaning with the convergence for m in FSM; In other words in case of small values of $m\pi/M$, we can see this relationship to check the accuracy of the results obtained by using FIT, comparing with the summation number M in FSM as shown in next article.

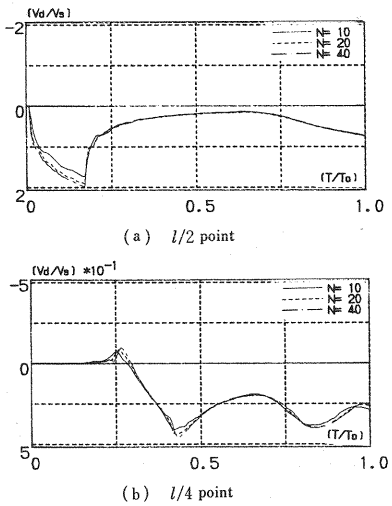

Fig. 13 Dynamic response of nondimensional vertical displacement V_d/V_s on the upper side versus nondimensional time period T/T_0.

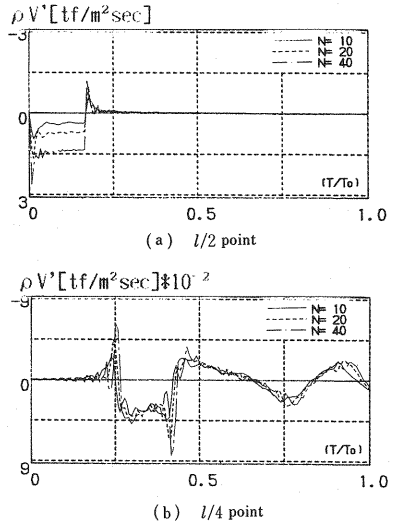

Fig. 14 Dynamic response of modified vertical velocity $\rho V'$ on the upper side versus nondimensional time period T/T_0.

(2) Comparison of dynamic response with different division number

In order to compare the dynamic response of the beam in the case of different vertical division numbers, the displacements and velocities of the beam in three cases of $N=10$, 20 and 40, are calculated. The beam is a simply supported homogeneous deep beam with unit thickness, 70 cm length, and 40 cm height as shown in Fig. 1 and is subjected to an impulsive step point load at the span center of the upper side with duration of 50 μs. Material constants are

$\mu=128\,200$ kgf/cm^2 (12.82 GPa), $\lambda=52\,520$ kgf/cm^2 (5.252 GPa), $M=80$, $\rho=0.2347$ g/cm^3, $\rho_f=A_f=0$.

The dynamic responses of vertical displacement at the middle and quarter points of upper side are shown in Fig. 13. The ordinate of this figure is normalized by the static displacement V_s at the span center of neutral axis subjected to static load P_0 and the abscissa is normalized by the time T_0 in which the shear wave reflects at a half length of the span and returns back.

Vertical velocities V' at the same points as in Fig. 13 are shown in Fig. 14 which is indicated by momentum unit $\rho V'$.

In Fig. 15, the vertical velocities at the $l/2$ and $l/4$ points of lower side are shown. Within the elapsed time of 50 μs of the impulse load ($T/T_0<0.2$), the small differences of velocity response at the upper side of the beam are found among three different cases of vertical division. But the other results in Fig. 14 (b) and Fig. 15 have no significant differences by the change of the vertical division number.

Next, to know the effect of longitudinal division number on the dynamic response, three different cases of $M=30$, 50, 100 are considered. The other values are taken as the same as in the above and $N=20$. The dynamic responses of vertical velocities at the $l/2$ and $l/4$ points of upper side are shown in Fig. 16. The effects of different longitudinal division number on the response in the elapse time of impulse load are found somewhat like those we get in vertical division as shown in Fig. 14.

(3) Comparison of the response of composite rectangular beam between theoretical and experimental results

To compare the impulse response of the composite rectangular beam between theoretical and experimental results, we take the mortar specimen reinforced by the fibers of one layer, as shown in Fig. 17. The following values are used in theoretical calculation. Material constants are

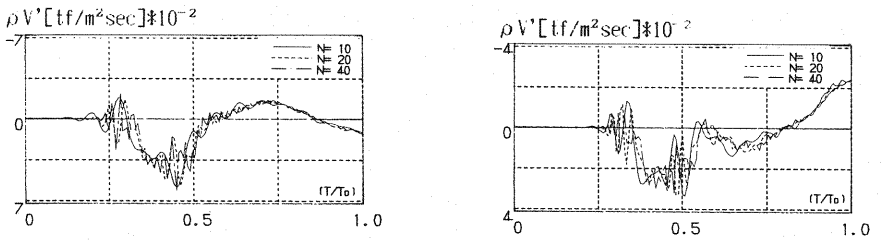

(a) $l/2$ point　　(b) $l/4$ point

Fig. 15 Dynamic response of modified vertical velocity $\rho V'$ on the lower side versus nondimensional time period T/T_0.

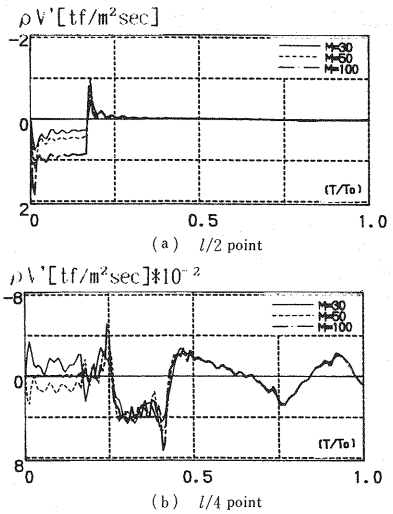

(a) $l/2$ point

(b) $l/4$ point

Fig. 16 The effect of longitudinal division number on modified vertical velocity $\rho V'$ on the upper side versus nondimensional time period T/T_0.

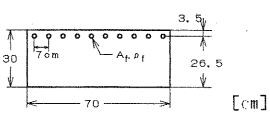

Fig. 17 The composite rectangular beam.

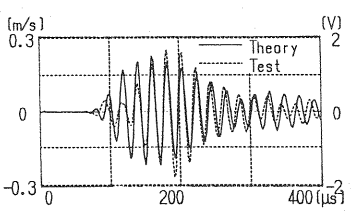

Fig. 18 Comparison of the impulse response of the velocity between theoretical and experimental results at $l/2$ point of lower side.

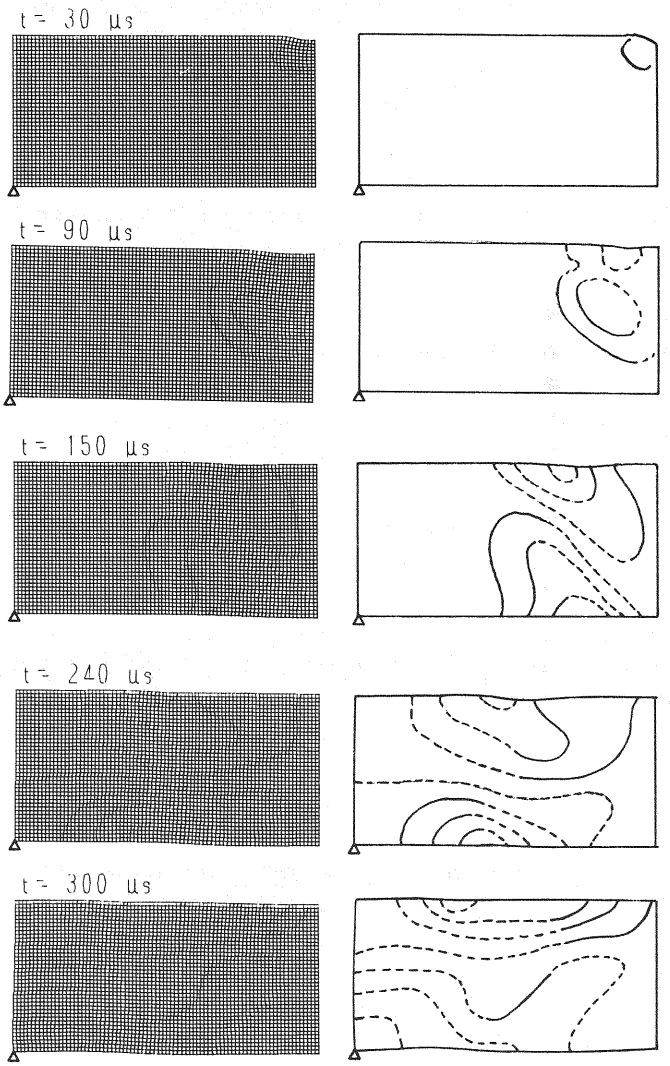

Fig. 19 Numerical simulation of stress wave propagation.

μ=85 470 kgf/cm² (8.547 GPa), λ=35 012 kgf/cm² (3.5012 GPa),
ρ=0.2347 g/cm³, ρ_f=0.801 g/cm³, A_f=2.835 cm²
The damping coefficient h_r is taken as in Eq. (14), and a=2 787 and b=9.0.

As the external point load of impulse at the $l/2$ point of upper side of the beam, the result shown in Fig. 6 is used. The contact pressure between a sensor and a beam is taken around 3 kgf/cm^2. Comparison between theoretical and experimental results of the velocity is shown in Fig. 18 at the $l/2$ point of lower side. The ordinate of the left hand side is taken for the theoretical result of velocity shown in Fig. 18 by solid line. The experimental result of the velocity is obtained as a change of voltage as shown in Fig. 18 by the dotted line and the ordinate of the right hand side is taken for this dotted line.

The abscissa means an actual passage time in microsecond. We can see the good agreement between theoretical and experimental results in Fig. 18.

(4) Numerical simulation of stress wave propagation

The impulsive incident wave applied at the span center of upper side propagates rapidly in the beam as transient stress wave and then whole oscillation modes appear successively along with the reflected waves from the beam boundary. These behaviors on the stress wave propagation are shown by the numerical simulations in Fig. 19. In this calculation the following values are utilized;

$T_p=50\ \mu$s (duration of impulse), $N=40$, $M=80$, $2C=6$ cm (loading length)

and the other values are taken as the same as in the above. The results shown in Fig. 19 are obtained by combining vertical and longitudinal components of displacement as the time history of propagation. In this case, the time in which dilatational wave returns back from the lower side of the beam is around 70 μs after the incident. From these figures we can see that the stress wave propagates in the beam in the elapsed time and the transient wave mode is gradually transformed into the whole oscillation mode. When the elapsed time of the incident is longer than the natural oscillation period of the beam, the dynamic response may take place as the history of whole oscillation of the beam just after the incident. From these visual simulation we can investigate the diffraction behavior of the transient stress wave propagating in the beam in which internal cracks or inclusions are involved.

6. CONCLUSION

Summarizing the above study on the stress wave propagation in the rectangular beam, we have come to the conclusions as follow;

(1) Taking into account the effects of impedance ratio between the transducer and the beam, the natural frequency of the transducer, and the contact pressure to the surface of the beam, the surface responses due to the incident stress wave applied by a piezoelectric transducer are measured by the ultrasonic pulse method.

(2) By dealing with the initial damping effect of the stress wave in the vicinity of impulse, the characteristics of phase shift caused by internal friction and the frequency dependence on damping coefficient are obtained by experiment.

(3) By the numerical models of the rectangular beam, the effects of mesh division of vertical and longitudinal directions are presented on the impulse response.

(4) The good agreement on the impulse response of composite rectangular beam of the velocity by the comparison between theoretical and experimental results is obtained as shown in Fig. 18.

(5) The transition process from the transient wave to the oscillation over the whole span of the beam is simulated by the numerical analysis.

Although results are not yet sufficient to apply the stress wave analysis as the diagnosis of the structural integrity, we wish to improve the accuracy of the diagnosis by continuing the study on the stress wave scattering.

ACKNOWLEDGMENTS

This study was supported partly by a Grant-in-Aid for Scientific Research from Japanese Ministry of Education, Science and Culture. The authors wish to thank Messrs. K. Watanabe, Y. Nakamura and H.

Yamamoto, former students of Kitami Institute of Technology, for their help in experimental study.

REFERENCES

1) Krautkramer, J. and Krautkramer, H. : Ultrasonic Testing of Materials, Third, revised Ed., Springer Verlag, 1983.
2) Nicholas, J. C., Sansalone, M. and Hsu, H. H. : A Point Source-Point Receiver, Pulse-Echo Technique for Flaw Detection in Concrete, ACI Journal, March-April, 1986.
3) Aloppi, A. and Mayer, W. G. : Ultrasonic Methods in Evaluation of Inhomogeneous Materials, NATO ASI Series, Martinus Nijhoff Publishers, 1987.
4) Ohtsu, M. : Source Inversion of Acoustic Emission Waveform, Structural Eng./Earthquake Eng., Vol. 5, No. 2, pp. 275 s-283 s, Oct. 1988.
5) Ohtsu, M., Yuyama, S. and Imanaka, T. : Theoretical Treatment of Acoustic Emission Sources in Microfracturing due to Disbonding, J. Acoust. Soc. Am., Vol. 82, No. 2, pp. 506-512, 1987.
6) Oshima, T., Mikami, S., Nomachi, S. G. and Kida, T. : Stress Wave Propagation in a Rectangular Composite Beam, Proc. of Fourth Japan-U. S. Conference on Composite Materials, Washington, D. C., 1988.
7) Oshima, T., Mikami, S., Nomachi, S. G. and Shigekiyo, K. : Stress Wave Velocity Propagating in Composites and its Application to Soundness Evaluation of Structures, Journal of Structural Eng., Vol. 32 A, 1986 (in Japanese).
8) Cheung, Y. K. : Finite Strip Method in Structural Analysis, Pergamon Press, 1976.
9) Kolsky, H. : Stress Waves in Solids, Dover Publications, 1963.
10) Granick, N. and Strern, J. E. : Material Damping of Aluminum by a Resonant-Dwell Technique, NASA TN D-2893, 1965.
11) Harris, C. M. and Crede, C. E. : Shock and Vibration Handbook, Vol. 1, 2-15, 1961.
12) Nomachi, S. G. and Matsuoka, K. G. : Applications of Finite Fourier Integration for Structural Mechanics, Theoretical and Applied Mechanics, Vol. 20, pp. 117-123, 1970.

(Received June 19 1989)